Nanoscale

Accepted Manuscript

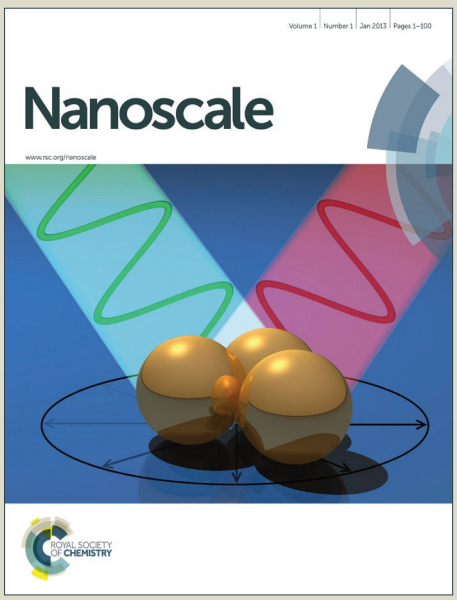

ROYAL SOCIETY OF CHEMISTRY

www.rsc.org/nanoscale

Journal Name

ARTICLE

Hydrophilic CeO_2 Nanocubes Protect Pancreatic β-cell Line INS-1 from H_2O_2-Induced Oxidative Stress

Received 00th January 20xx,
Accepted 00th January 20xx

DOI: 10.1039/x0xx00000x

www.rsc.org/

Guang-Ming Lyu,[a] Yan-Jie Wang,[a,c] Xue Huang,[b] Huai-Yuan Zhang,[a] Ling-Dong Sun,[a,*] Yan-Jun Liu[b,*] and Chun-Hua Yan[a,*]

Oxidative stress plays a key role in the occurrence and development of diabetes. With its unique redox property, CeO_2 nanoparticles (nanoceria) exhibit promising potential for the treatment of diabetes resulting from oxidative stress. Here, we develop a novel preparation of hydrophilic CeO_2 nanocubes (NCs) with two different sizes (5 nm and 25 nm) *via* an acetate assisted hydrothermal method. Dynamic light scattering, zeta potential measurements and thermogravimetric analyses were utilized to investigate the changes in physico-chemical characteristics of CeO_2 NCs when exposed to *in vitro* cell culture conditions. CCK-8 assays revealed that the CeO_2 NCs did not impair cell proliferation in the pancreatic β-cell line INS-1 at the highest dose of 200 μg/mL over the time scale of 72 h, while being able to protect INS-1 cells from H_2O_2-induced cytotoxicity even after protein adsorption. It is also noteworthy that nanoceria with a smaller hydrodynamic radius exhibits stronger antioxidant and anti-apoptotic effects, which was consistent with their H_2O_2 quenching capability in biological system. These findings suggest that nanoceria can be used as an excellent antioxidant for controlling oxidative stress-induced pancreatic β-cell damage.

Introduction

Due to the pronounced changes of human's living habit and lifestyle, diabetes has become a main threat to human health.[1,2] It is estimated that the number of people suffering from diabetes worldwide is expected to rise to 552 million by 2030.[3] Oxidative stress, induced by the increased biological production of reactive oxygen species (ROS), plays a central role in the development of hyperglycemia-induced diabetic complications.[4,5] Unfortunately, pancreatic β-cells are particularly susceptible to ROS because they have a low level of expression of antioxidant enzymes.[6] Therefore, effective and controllable antioxidants to reduce oxidative stress-induced damage in pancreatic β-cells are required in the treatment of diabetes mellitus.[7,8]

CeO_2 is one of the most important functional materials that have been used in many fields, for example, heterogeneous catalysts,[9-11] gas sensors,[12] UV filters,[13] and solid oxide fuel cells.[14] More recently, nanoceria have received considerable attention as they can act as free radical scavengers in many biological contexts derived from the redox processes on the nanoparticle surface.[15] It has been reported that nanoceria exhibit superoxide dismutase SOD mimetic activity,[16,17] catalase mimetic activity,[18] and hydroxyl radical scavenging activity[19] to eliminate excessive ROS. Initial biological studies indicate the great potential of nanoceria for controlling oxidative stress-related fields including cancer, retinal degeneration, ischemic stroke, chronic inflammation, neurological disorders, even plant biology.[20-28]

The physiochemical properties of nanoceria (size, morphology, agglomeration state, surface charge, surface coating and surface oxidation state) have a remarkable impact on their antioxidant performances.[29-33] Thus, CeO_2 NCs enclosed by highly reactive {200} planes with controlled size are quite desirable.[34,35] Among many reported approaches for controlling the growth of nanoceria, hydrothermal method with the use of surfactants or organic templates, is regarded as one of the most effective routes.[36,37] However, the residual conventionally-used chemical additives may contaminate the CeO_2 NCs and limit their bio-applications. Therefore, the synthesis of CeO_2 NCs with exposed {200} facets using biocompatible capping regents are suitable for bio-antioxidation.

It is now well-recognized that certain proteins and other biomolecules will drastically be adsorbed onto the surface of nanoparticles when they enter a biological medium, forming a bio-nano interface described as "protein corona".[38,39] In fact, it has been found in a series of *in vivo* and *in vitro* studies, including toxicological tests and final biomedical applications, that it is the formed nanoparticle-corona conjugates that act as the biological active species.[40-42] Therefore, a better understanding of the interaction between nanoceria and the

[a] *Beijing National Laboratory for Molecular Sciences, State Key Laboratory of Rare Earth Materials Chemistry and Applications, PKU-HKU Joint Laboratory in Rare Earth Materials and Bioinorganic Chemistry, College of Chemistry and Molecular Engineering, Peking University, Beijing 100871, China. Fax: +86-10-62754179; Tel: +86-10-62754179; Email: sun@pku.edu.cn, yan@pku.edu.cn*
[b] *Department of Endocrinology, 306 Hospital of People's Liberation Army, Beijing 100101, China. Email: damaoermaosanmao@aliyun.com*
[c] *Key Laboratory for Advanced Battery Materials and System (MOE), School of Materials Science and Engineering, Huazhong University of Science and Technology (HUST), Wuhan, Hubei 430074, China*
† Electronic Supplementary Information (ESI) available. See DOI: 10.1039/x0xx00000x

physiological medium is extremely essential. In previous works the formation mechanism and time evolution of protein adoption onto CeO_2 nanoparticles have been studied.[43,44] However, few studies have focused on how the nanoparticle size and surface properties of nanoceria affect the formation of protein corona, which can bring greatly changes to their antioxidant performances.

In this study, we develop a facile acetate assisted hydrothermal method for obtaining highly-crystallized CeO_2 NCs. Both the shape and size of nanoceria were controlled by varying cerium precursors and reaction conditions. Efforts have been made to understand the effects of cell culture media on the physical, chemical and biological properties of CeO_2 NCs, using zeta potential measurements, dynamic light scattering, thermogravimetric analysis, UV-vis spectroscopy and catalase mimetic activity assay. Furthermore, INS-1 pancreatic β cells were employed to evaluate the cytotoxicity and potential antioxidant properties of the as-prepared CeO_2 NCs.

Experimental

Synthesis of CeO_2 NCs

Small-sized CeO_2 NCs with the size of 5.0 ± 0.8 nm (denoted as CeO_2-5 NCs) were prepared from the hydrolysis of $(NH_4)_2Ce(NO_3)_6$ in an acetate-acetic acid buffer system under hydrothermal conditions. In a typical procedure, 10 g sodium acetate and 10 mL pure acetic acid were dissolved in 50 mL water to form buffer solution. 5 mmol $(NH_4)_2Ce(NO_3)_6$ was dissolved in the buffer solution and stirred for about 10 min. The solution was then diluted to 85 mL and transferred into a 100-mL Teflon-lined stainless steel autoclave and heated to 220 °C for 24 h. After being cooled to room temperature, the precipitates were collected by centrifugation, and washed with distilled water for five times. Finally, the products were dispersed in water to generate stable nanoceria colloid solutions.

Large-sized CeO_2 NCs with the size of 25.0 ± 6.6 nm (denoted as CeO_2-25 NCs) were obtained from the hydrolysis of $Ce(NO_3)_3$. Other reaction conditions and aftertreatments are the same as aforementioned.

Characterization of CeO_2 NCs

X-ray diffraction (XRD) analysis were performed on a Rigaku D/MAX-2000 diffractometer (Japan) operated at 40 kV and 100 mA, with a slit of 0.5 ° and a scanning speed of 8 °/min, equipped with a Cu Kα radiation source (λ = 0.15418 nm). Transmission electron microscopy (TEM) images were taken on a JEOL JEM-2100 TEM (Japan) under the working voltage of 200 kV. High-resolution TEM (HRTEM) analyses were performed on a JEOL JEM-2100F TEM (Japan) operated at 200 kV. The Brunauer-Emmett-Teller (BET) specific surface area (SBET) was measured by nitrogen adsorption at 78.3 K, using an ASAP 2010 analyzer (Micrometritics Co. Ltd.) after samples were evacuated ($<10^{-3}$ Torr) at 373 K for 8 h. X-ray photoelectron spectra (XPS) experiments were performed on an Axis Ultra imaging photoelectron spectrometer (Kratos Analytical Ltd., U.K.). The photoelectron spectrometer utilized an Al Ka (1486.6 eV) anode operating at 100 W. The base pressure during XPS analysis was maintained at less than10^{-9} mbar, and the binding energy scale was calibrated by the C 1s peak at 284.8 eV. Raman spectra were measured on a Jobin–Yvon HR800 Laser Raman Microscope with an excitation wavelength of 514 nm. Signals were recorded using the extended measurement mode in the range 100-2000 cm^{-1} with 10 accumulations and 1800 L/mm grating. A Bruker Vector22 Fourier-transform infrared (FT-IR) spectrometer (Germany) was used to measure the surface chemical structure of the as-prepared nanoceria, with signals recorded between 400 and 4000 cm^{-1}.

Characterization of CeO_2 NCs in different dispersion media

CeO_2 NCs were dispersed in different media (water, RPMI 1640 medium or RPMI 1640 medium with 10% fetal bovine serum (FBS)), and the hydrodynamic radius distribution was measured with an ALV/DLS/SLS5022F light scattering-apparatus equipped with a 22 mW He-Ne laser (632.8 nm wavelength). A Zetasizer Nano ZS90 (Malvern) instrument was used to measure the zeta potential (surface charge) of CeO_2 NCs (both as-prepared and after incubation with RPMI-1640 + 10% FBS for 24 h) loaded into a pre-rinsed folded capillary cell at 25 °C. The thermogravimetric analysis (TGA) experiments of the powdered samples (both as-prepared and after incubation with RPMI-1640 + 10% FBS for 24 h) were performed using Q600SDT (TA, USA) under an air atmosphere, at a flow rate of 100 mL/min. The data was recorded from ambient temperature up to 600 °C with the heating rate of 10 °C/min.

Protein adsorption to CeO_2 NCs surface

The as-prepared CeO_2-5 NCs and CeO_2-25 NCs colloid solutions (2 mg/ml) were mixed with RPMI-1640 medium + 10% FBS. Then the mixture was sonicated for 30 s and placed in an incubator at room temperature for 24 h. Centrifugation (3 times) was used for the separation of the nanoparticle-protein conjugates from unbound proteins.

Catalase mimetic activity assay

The catalase mimetic activity assay of CeO_2 NCs (before and after incubation with RPMI-1640 + 10% FBS for 24 h) was carried out in 96 well plate. Aqueous H_2O_2 solution was prepared using ultrapure water and commercial 30 v/v% H_2O_2, and titrated by $KMnO_4$ before use. 80 μL H_2O_2 solution (100 μg/mL) and 20 μL nanoceria stock solution (250 μg/mL) was added to each well. The conversion of H_2O_2 was detected by the observed colour change upon the addition of 20 μL H_2SO_4 (6 mol/L) and 80 μL $KMnO_4$ (2 mmol/L) standard solution, and determined using absorption spectroscopy. The absorbance at a wavelength of 525 nm was detected on Bio-Tek Synergy 4 multi-mode microplate reader. All experiments were carried out in sextuplicate.

Cell culture

INS-1 cells, a rat insulinoma cell line, were purchased from the National Platform of Experimental Cell Resources for Sci-Tech (China). The cells were cultured in RPMI-1640 medium

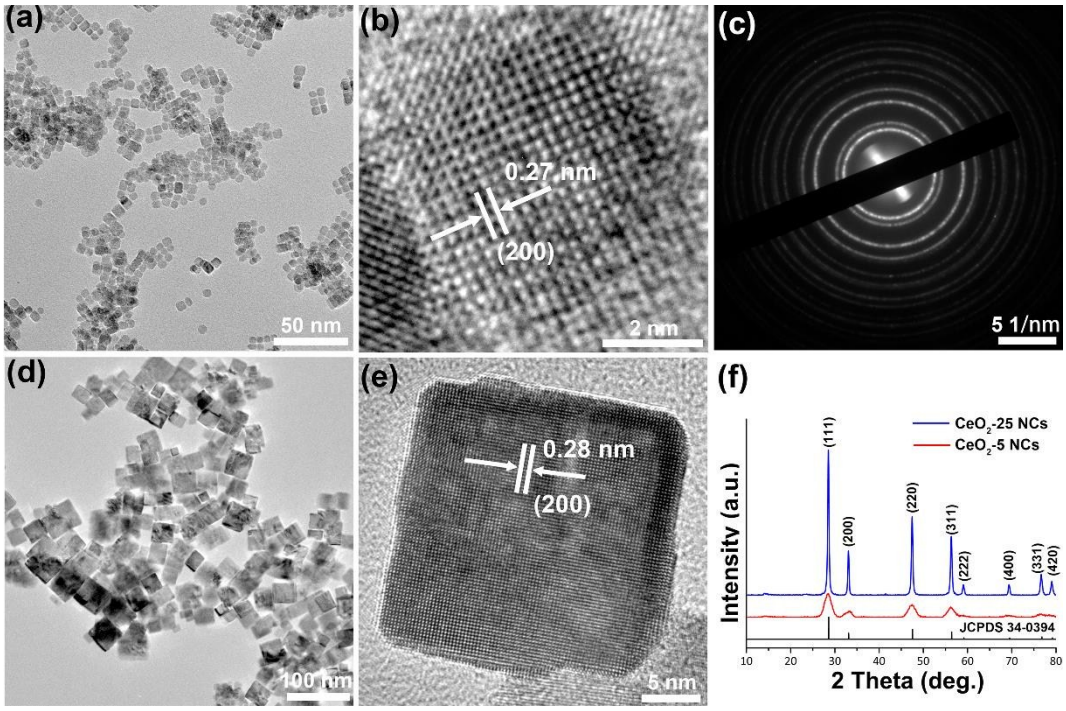

Fig. 1 TEM image (a), HRTEM image (b) and SAED image (c) of the as prepared CeO_2-5 NCs. TEM image (d) and HRTEM image (e) of CeO_2-25 NCs. Powder XRD patterns (f) of CeO_2-5 NCs and CeO_2-25 NCs.

supplemented with 10% fetal bovine serum, 1 mmol/L sodium pyruvate, 50 µmol/L 2-mercaptoethanol, 100 IU/mL penicillin and 100 µg/mL streptomycin. The medium was changed every 2–3 days and 24 h before adding nanoparticles to be tested. All experiments were incubated at 37 °C in a humid atmosphere (5% CO_2, 95% air).

Cytotoxicity of CeO_2 NCs

The biosafety of nanoceria was evaluated using CCK-8 assay (Dojindo, Kumamoto, Japan), based on the reduction of tetrazolium salt to formazan by dehydrogenases in living cells. Briefly, 1.5×10^4 cells per well in 120 µL was plated into a 96-well plate and pre-incubated for 24 h at 37 °C and 5% CO_2 atmosphere. Then, 6 µL CeO_2 NCs colloid solution with various sizes and concentrations were added to the 96-well plate. The cells viability was analyzed at 24, 48 and 72 h after the addition of nanoceria, when the cells were removed from the culture media and then washed with PBS. 10 µL CCK-8 solution and 90 µL fresh culture medium were added to each well, and the 96-well plate was incubated for additional 2 h. The absorbance at 450 nm and a reference wavelength of 650 nm were detected on Bio-Tek Synergy 4 multi-mode microplate reader. All experiments were carried out in sextuplicate.

Quantification of intracellular CeO_2 NCs in INS-1 cells

INS-1 cells were seeded in a 6-well plate (5×10^5 cells/well), and cultured for 2 days at 37 °C under 5% CO_2 atmosphere. Then the culture medium was removed and replaced with fresh medium containing 100 µg/mL 5 nm or 25 nm CeO_2 NCs. After 24 h incubation, the cells were washed two times with PBS (pH 7.4), trypsinized, centrifuged and digested with 1 mL concentrated nitric acid. Finally, the concentration of cerium was analyzed using inductively coupled plasma-atomic spectroscopy (ICP-AES, Leeman, U.S.A.). Each experiment was performed thrice and consistent data were obtained.

Apoptosis Induction and cell viability assay

Direct exposure to dilute H_2O_2 can induce the apoptosis of INS-1 cells *in vitro*, which can be used as a valuable apoptotic model to study the mechanism of oxidative injury. In our study, INS-1 cells were initially seeded in 96-well plates at a density of 1.5×10^4 cells per well in 120 µL and were cultured for 72 h at 37 °C in a 5% CO_2 atmosphere. H_2O_2 solution were freshly diluted from a 30% stock solution, and then 6 µL H_2O_2 solution (10 mM) was directly added to each well. After 1 h incubation and the following wash with PBS, the cells were placed in fresh media for recovery to allow apoptosis. CeO_2 NCs with different concentrations were added into each well. After the treatment for 24 h, CCK-8 assay was used for the determination of the cell viability as described above.

Statistical analysis

Results were expressed as the mean ± standard error of mean. Data were analyzed by Student *t* test or ANOVA. A *P*-value of less than 0.05 ($P < 0.05$) was considered to be statistically significant.

Results and discussion

Characterization of CeO_2 NCs

The aqueous dispersions of CeO_2 NCs of different sizes were obtained from the hydrolyzation of $(NH_4)_2Ce(NO_3)_6$ or $Ce(NO_3)_3$ in an acetate-acetic acid buffer under hydrothermal condition. The average sizes of these two CeO_2 NCs are 5.0 ± 0.8 nm (obtained from Ce(IV) precursor) and 25.0 ± 6.6 nm (obtained from Ce(III) precursor), respectively. Accordingly, the two types of CeO_2 NCs were denoted as CeO_2-5 NCs and CeO_2-25 NCs, respectively (Fig. S1, ESI†). Fig. 1a and 1b show the TEM and HRTEM images of CeO_2-5 NCs. The clear lattice fringes across

the particle indicate the high crystallinity of the products, and the 0.27 nm interplanar spacing suggests the exposure of {200} plane. The selected area electron diffraction (SAED) pattern also indicates that the NCs are well-crystallized (Fig. 1c). From TEM and HRTEM image of the CeO_2-25 NCs in Fig. 1d, e, high-crystallinity and exposed {200} plane can also be observed. XRD patterns of CeO_2-5 NCs and CeO_2-25 NCs are depicted in Fig. 1f, and their diffraction patterns correspond well to the standard patterns of referenced CeO_2 with *fcc* structure (JCPDS 34-0394, space group $Fm\overline{3}m$).

The presence of acetate ions in the reaction system was found essential for the successful synthesis. The hydrolysis of cerium precursor towards the formation of nanoceria is a process with protons production. However, acetate ions consumed the H^+ released during the reaction, to keep the pH value at a nearly constant between 4.5 and 4.6 during the growth of the nanoceria. This relative stable environment is considered to be a necessary condition for the size uniformity and the relative high yield of products. In addition, the acetate ions also functioned as the special capping reagent to control the size and shape of nanoceria.[36,45,46] When the amount of the buffer decreased to 2 mL HAc and 2 g NaAc per reaction vessel, and kept other conditions, only inhomogeneous irregular particles could be produced.

It was found that the oxidation state of cerium in precursor played the key role in determining the size of as-prepared CeO_2 NCs.[47,48] As known, the solubility product of $Ce(OH)_4$ (2×10^{-48}) is significantly lower than that of $Ce(OH)_3$ (1.6×10^{-20}).[45] Ce(IV) salts usually undergo strong hydration, leading to a larger number of nuclei which favors the formation of small size CeO_2 nanocrystals. When $(NH_4)_2Ce(NO_3)_6$ is replaced by $Ce(NO_3)_3$, an oxidation conversion from $Ce(OH)_3$ intermediates to CeO_2 species by $NO3^-$ ions becomes necessary.[49] Because the additional step is slower than hydrolysis, the Ce(IV) concentration can only be partially compensated by the oxidation of Ce(III) after the nucleation process, thus, favouring the further growth and restraining the Ostwald ripening process. As a result, large-sized CeO_2 NCs formed.

Raman spectroscopy was employed to analyze the surface property of CeO_2 NCs. As depicted in Fig. 2a, only main peak at ~465 cm^{-1} can be observed. This peak is attributed to the F_{2g} mode vibration in fluorite-structure lattice (space group O_h). Importantly, this peak was observed to be more asymmetric in shape and appeared at lower wavenumbers for the smaller CeO_2-5 NCs. Moreover, the full width at half-maximum (HWHM) of the peak increased with the decreasing particle size (10.9 cm^{-1}, 18.3 cm^{-1}, and 40.6 cm^{-1} for micro, CeO_2-25 and CeO_2-5 NCs, respectively).

To investigate the oxidation state (Ce(III)/Ce(IV) ratio) of Ce ions on the surface of CeO_2 NCs, XPS analysis was performed.[50] In previous studies, the Ce(III)/Ce(IV) ratio was found to be dependent on the particle size of ceria.[51,52] However, in this work, we noticed a distinctive phenomenon. The Ce 3d spectra of the two samples almost coincide with the standard Ce(IV) spectrum (Fig. 2b). The detailed analysis of Ce 3d XPS spectra are shown in Fig. S2†. Specifically, the Ce(III)/Ce(IV) ratio is about 3% and 2% for CeO_2-5 NCs and CeO_2-25 NCs, respectively. The extreme low levels of Ce(III) could be attributed to the high crystallinity of as-prepared CeO_2 NCs (5 nm and 25 nm) with few surface oxygen defects.

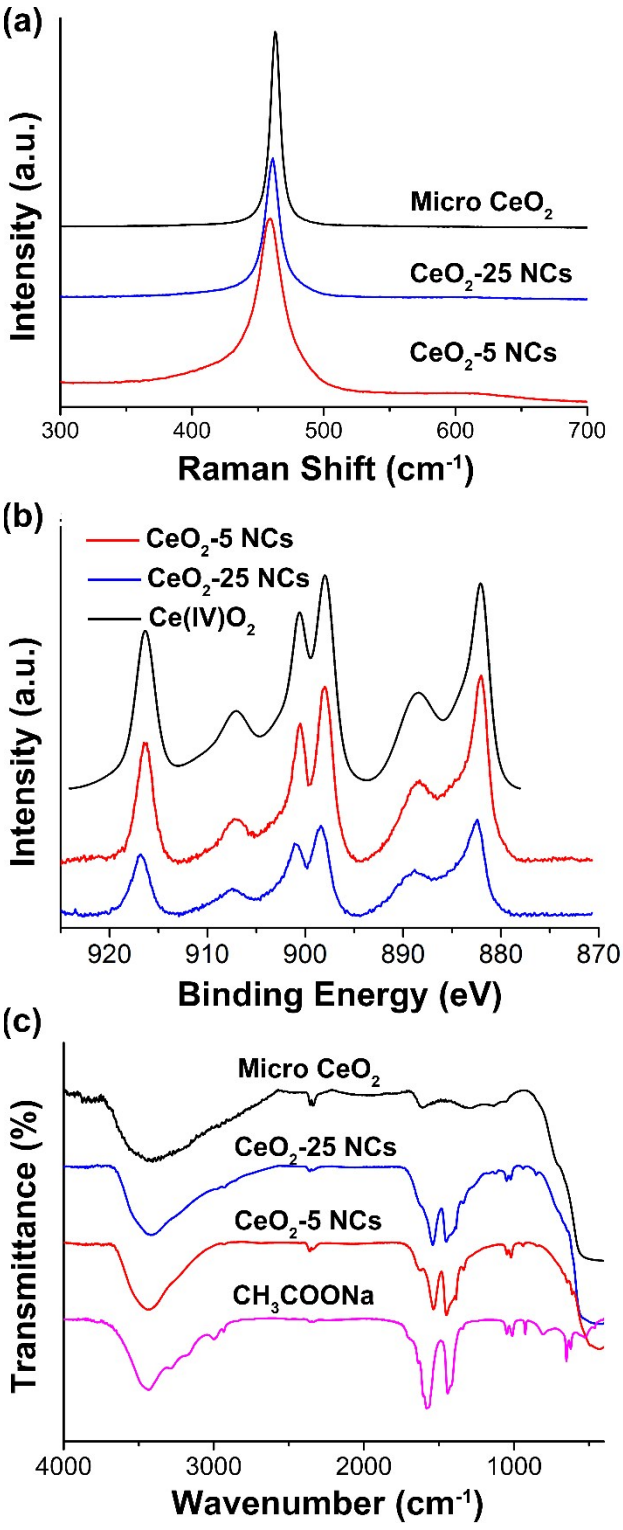

Fig. 2 (a) Raman spectra of different-sized CeO_2. (b) Ce 3d XPS patterns to identify the surface oxidation state of Ce ions. (C) FT-IR analysis of acetate-stabilized CeO_2 NCs.

FT-IR spectra of the nanoceria were collected between 400 and 4000 cm^{-1} (Fig. 2c). An intense and broad band centered at 3400 cm^{-1} revealed the presence of adsorbed water in all the samples. The band at 1535 cm^{-1} was attributed to the COO^- antisymmetric stretch, and that at 1450 cm^{-1} was related to the COO^- symmetric stretch, both of which suggested the presence of acetate ions on the surface of nanoceria. Compared with the signal of CH_3COONa, a large red-shift of carbonyl absorption band was observed, indicating the strong metal-ligand interactions between cerium and acetate species.

Influence of *in vitro* cell culture conditions on the physico-chemical characteristics of CeO_2 NCs

In a biological environment, some important nanoparticle properties, such as surface charge (zeta potential), hydrodynamic diameter, particle aggregation, are determined by the ionic strength, pH, and the presence of biomolecules (for example proteins) of a given medium.[53] Understanding the interfacial interactions between nanoceria and complex biological fluids are essential for their potential biomedical applications. Therefore, we have followed the changes of the physical properties of CeO_2 NCs when exposed to cell culture medium (RPMI-1640 supplemented with 10% FBS) for 24 h. Moreover, physical-chemical factors that affect the nature of nanoceria-protein coronas, including particle size, surface charge, and specific surface area, were carefully investigated.

Nanoceria dispersions with a high colloidal stability is prerequisite for extended biological applications. As shown in Fig. S3†, no sediment was observed in DI water dispersion of CeO_2 NCs, even for several months. Zeta potential measurements revealed that the as-prepared CeO_2 NCs were positively charged (+47/+45 mV for CeO_2-5 NCs/CeO_2-25 NCs). The electrostatic repulsion forces between colloid particles facilitate the colloid stability of the resulting suspension. Subsequently, the hydrodynamic radii of the acetate-stabilized CeO_2 NCs with various treatments were tested by DLS (Fig. 3). In the as-prepared CeO_2 water colloidal solutions, the intensity-weighted average particle radius was 24 nm and 49 nm for CeO_2-5 NCs and CeO_2-25 NCs, respectively.

The samples were incubated with RPMI 1640 medium without serum for 24 h for further analysis. The hydrodynamic radius increased to 319 nm and 252 nm, respectively. In the meanwhile, the mean particle surface charge (zeta potential) of the CeO_2-5 NCs decayed from a +47 mV to 0 mV, and for CeO_2-25 NCs. the value changed from +45 mV to a negative value of -2 mV (Table S1†). The change in zeta potential should be attributed to the prominent elimination of coulombic repulsion in initial colloidal solution, which was responsible for stabilizing nanoceria, by inorganic ions in the culture medium. As a result, significant aggregation of nanoceria occurred, especially for small-sized CeO_2-5 NCs.

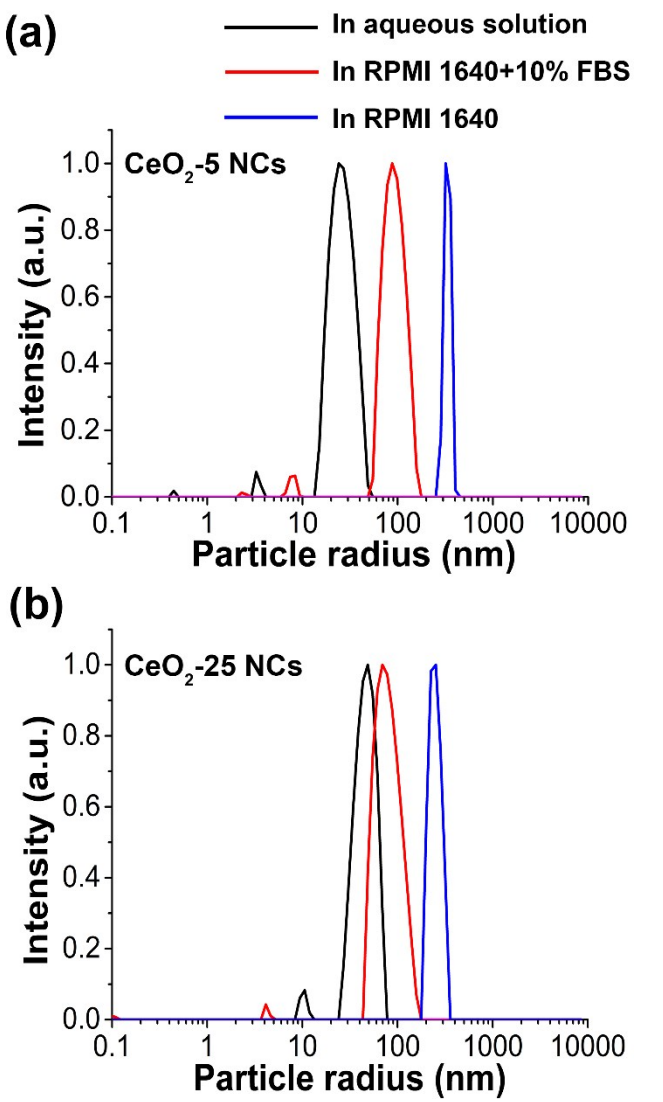

Fig. 3 Hydrodynamic size distributions of CeO_2-5 NCs (a) and CeO_2-25 NCs (b) in different media

Nevertheless, when the CeO_2 NCs were added to the RPMI 1640 medium complemented with 10% FBS, the nanoparticles displaying positive surface charges readily adsorbed negatively charged proteins via Coulomb interactions. The zeta potential decreased to 0 mV and -3 mV and the hydrodynamic

Table 1 Physicochemical parameters of the as-prepared CeO_2 NCs in different media.

Sample	TEM diameter (nm)	Hydrodynamic radius (nm)			zeta potential (mV)		
		In aqueous solutions	In RPMI 1640	In RPMI 1640 + 10% FBS	In aqueous solutions	In RPMI 1640	In RPMI 1640 + 10% FBS
CeO_2-5 NCs	5	24	319	88	+47	0	0
CeO_2-25 NCs	25	49	252	69	+45	-3	-2

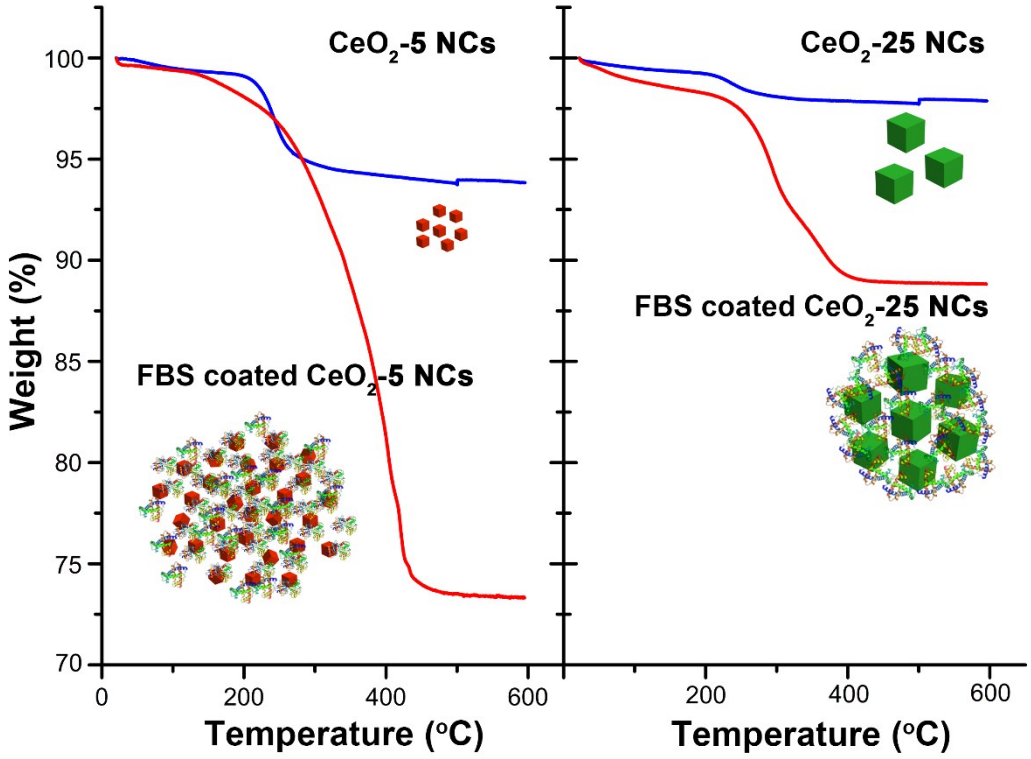

Fig. 4 Thermogravimetric curves for CeO_2-5 NCs (left panel) and CeO_2-25 NCs (right panel) before (blue line) and after (red line) incubation with RPMI-1640 + 10% FBS for 24 h.

radii increased to 88 nm and 69 nm for CeO_2-5 NCs and CeO_2-25 NCs, respectively (Fig. 3). Although the hydrodynamic radius of the as-prepared CeO_2 NCs increases due to the formation of nanoceria-protein conjugates, this protein corona effectively reduced the aggregation of colloidal CeO_2 NCs by changing their both electrical and steric properties. The aggregation degree of the nanoceria-protein corona conjugates was observed using TEM and bright-field mode of confocal microscopy. From the TEM images shown in Fig. S4†, the size of CeO_2 NCs aggregation unit after protein adsorption was larger than the as-prepared CeO_2 NCs, especially for small-sized CeO_2-5 NCs, but the confocal images showed that no sediment can be seen in cell culture media containing 10% FBS. In comparison, the CeO_2 NCs sedimentated seriously in RPMI 1640 medium without FBS, and obvious aggregates appeared (Fig. S5, ESI†).

Thermal gravity analysis (TGA) was further employed to probe the interaction between nanoceria and protein corona. As shown in Fig. 4, a total weight loss of 6% and 2% of the initial mass was observed for CeO_2-5 NCs and CeO_2-25 NCs, respectively. By contrast, after incubation with RPMI 1640 + 10% FBS during 24 h, more significant weight loss was noticed, with 26% and 11% for CeO_2-5 NCs and CeO_2-25 NCs, respectively, implying the protein absorption (Fig. 4). The amount of protein adsorbed on nanoceria particles (per gram) was calculated using following equation:

$$q = \frac{WL_1\% - WL_2\%}{1 - WL_1\%}\ g \qquad (1)$$

In Eq. (1), WL1% and WL_2% are the weight loss of CeO_2 NCs after incubation with RPMI 1640 + 10% FBS and as-prepared samples, respectively. A protein adsorption of 268 mg/g of nanoceria was obtained for the CeO_2-5 NCs while per gram of the CeO_2-25 NCs adsorbed 98 mg of protein. These values, together with the hydrodynamic radii from DLS data, suggested that the small-sized CeO_2-5 NCs with a larger hydrodynamic radius adsorbed much more protein than the CeO_2-25 NCs did.

Table S1† shows detailed physicochemical parameters of as-prepared and FBS-exposed nanoceria. Due to the same synthesis procedure, the two as-prepared samples have similar physicochemical properties, such as shape, surface defects, surface charge and surface coatings. Therefore, we can induce the particle size and surface area of CeO_2 NCs are crucial to the adsorption of protein. As the particles' size decreases, the surface area significantly increases. Smaller CeO_2 NCs are more efficient in species adsorption. The BET and TGA results showed that the amount of residual acetate or coating proteins on the surface of the CeO_2 NCs was nearly proportional to their surface area (Table S1†).

In vitro cytotoxicity and antioxidant properties of CeO_2 NCs

The biosafety of nanoceria is of great importance for extended treatments in oxidative stress-related diseases, such as neurodegenerative disorders, cancer and diabetes. To evaluate the cytotoxicity and potential antioxidant activity of the as-prepared CeO_2 NCs *in vitro*, INS-1 rat pancreatic β cells were employed in our studies. In the first step, we examined the cell viability of INS-1 cell line when incubated with the 5 nm CeO_2 NCs and 25 nm CeO_2 NCs for increasing concentrations and incubation times. CCK-8 assay revealed that compared to cells

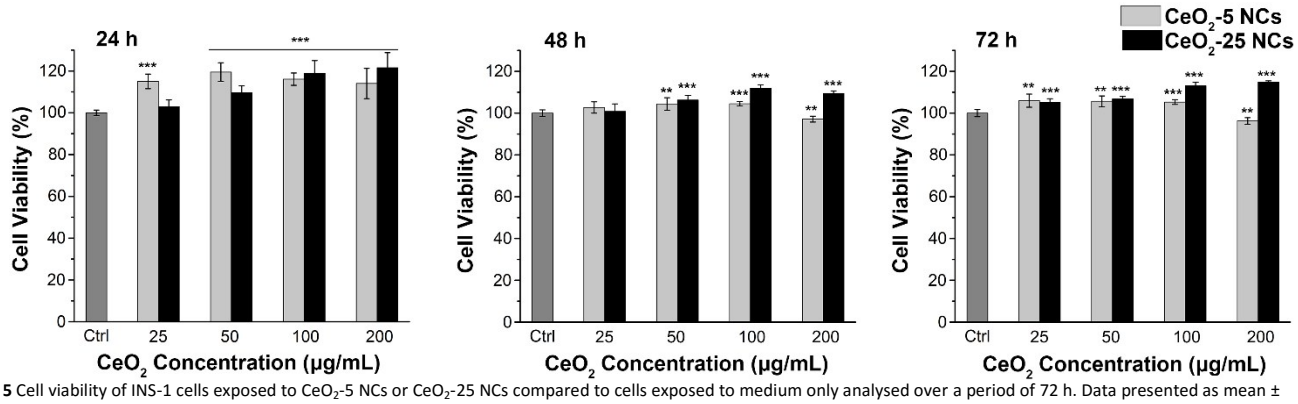

Fig. 5 Cell viability of INS-1 cells exposed to CeO_2-5 NCs or CeO_2-25 NCs compared to cells exposed to medium only analysed over a period of 72 h. Data presented as mean ± standard deviation (n = 6). $^{**}p < 0.01$, $^{***}p < 0.001$ vs. control group.

exposed to normal growth conditions, the CeO_2 NCs did not impair the proliferation of INS-1 cells at the highest dose of 200 μg/mL over the time scale of 72 h (Fig. 5). It is noteworthy that the cell viability of INS-1 cells was significantly increased with the presence of CeO_2 NCs within the first 24 h. Similar results for CeO_2 NCs-induced INS-1 cells proliferation were observed using another method of direct cell counting (Fig. S6, ESI†). This phenomenon should be attributed to the antioxidant properties of nanoceria.[25] The fluorescent signal of dichlorofluorescein (DCF) was analyzed to indicate intracellular ROS levels. The flow cytometry results showed that nanoceria could reduce basal intracellular free radicals level in a time-dependent manner. After 10 h exposure to 50 μg/mL CeO_2-5 NCs, intracellular ROS levels was reduced to approximately 33% of the medium control (Fig. S7, ESI†). Confocal images confirmed that the fluorescent signal of CeO_2 NCs-pretreated INS-1 cells was significantly diminished, suggesting a reduced ROS level (Fig. S8, ESI†).

The cellular internalization of as-prepared CeO_2 nanoparticles was also investigated. As shown in Fig. S9†, at incubation time of 24 h, both CeO_2-5 NCs and CeO_2-25 NCs can be internalized in INS-1 cells. Moreover, the amount of internalized CeO_2 nanoparticles was similar for CeO_2-5 NCs and CeO_2-25 NCs. As known, the cytotoxicity and internalization of nanoceria is affected by their physiochemical properties, including size and agglomeration degree, morphology, surface coating and surface charge. On this basis, the excellent cytocompatibility of CeO_2 NCs should be attributed to the clean and highly-effective synthetic method, which produces hydrophilic particles with narrow distributed size, well-defined morphology and non-residual surfactant on the surface. In addition, instantaneous protein adsorption tends to decrease the zeta potential of CeO_2 NCs towards the neutral, thereby preventing FBS-coated CeO_2 NCs from adhering onto the negatively charged cell surface, which is likely to mitigate the toxicity of the bare particles.[54-56]

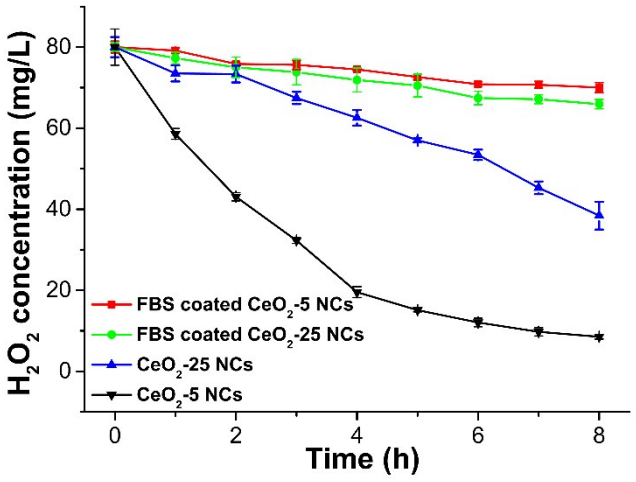

Fig. 6 H_2O_2 decomposition activity for CeO_2 NCs before and after incubation with RPMI-1640 + 10% FBS for 24 h.

It is well known that the intrinsic properties of nanoceria, such as the particle size, morphology, and concentration of oxygen vacancies, have a remarkable impact on its antioxidant performances.[29,32] However, few reports focused on the formation of protein corona and extended influence on the antioxidant properties of nanoceria. Here, the H_2O_2 decomposition activity of as-prepared and protein-coated CeO_2 NCs was evaluated (Fig, 6). The protein concentration adsorbed on CeO_2 NCs was much lower than the H_2O_2 concentration in the reaction system, which excluded the interference of protein oxidation by H_2O_2. The specific reaction rate at 37 °C and the turnover frequency (TOF) data are summarized in Table S2†. The results showed that CeO_2-5 NCs exhibited much higher catalase mimetic activity (25 $mmol \cdot h^{-1} \cdot g^{-1}$) than CeO_2-25 NCs (5.5 $mmol \cdot h^{-1} \cdot g^{-1}$). Nonetheless, after incubation with RPMI-1640 + 10% FBS, the nanoceria-protein corona conjugates formed from the CeO_2-25 NCs showed a higher catalytic activity (3.0 $mmol \cdot h^{-1} \cdot g^{-1}$) than those from the CeO_2-5 NCs (2.0 $mmol \cdot h^{-1} \cdot g^{-1}$).

It has been reported that the nanoceria's ability to mimic natural enzymes were associated with the total size (hydrodynamic diameter) of the nanoparticles.[57] From our analyses, a hydrodynamic radius dependent manner was found for nanoceria in mimicing catalase. The catalytic activity exhibited the variation trend as CeO_2-5 NCs (24 nm) > CeO_2-25 NCs (49 nm) > FBS-coated CeO_2-25 NCs (69 nm) > FBS-coated CeO_2-5 NCs (88 nm). The decrease in catalase mimetic activity of nanoceria-corona conjugates could be attributed to the less efficient interactions between the CeO_2 NCs and H_2O_2, which were further revealed by UV-vis absorption study. When the as-prepared colorless CeO_2 colloidal solution was treated with H_2O_2, the solution gradually turned yellow with the red-shift in

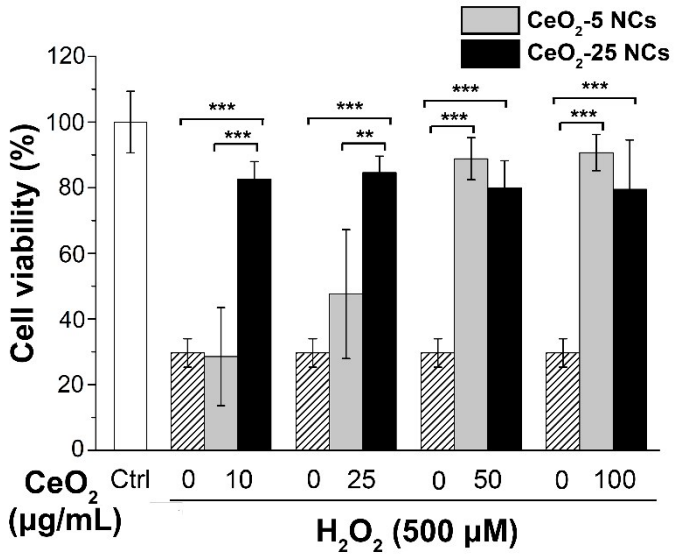

Fig. 7 Protective effects of CeO_2 NCs against H_2O_2-induced INS-1 cells apoptosis *in vitro*. Data presented as mean ± standard deviation (n = 6). $^{**}p < 0.005$, $^{***}p < 0.0001$ vs. other group.

its absorption spectrum.[58] However, this red-shift of absorbance band of the conjugate of nanoceria-corona were found weaker for the samples with bigger hydrodynamic radius (Fig. S10, ESI†), indicating that the protein corona can block the adsorption and desorption of oxygen from the nanoceria core surface. This observation also explains the prominent decrease in catalase mimetic activity for small-sized CeO_2-5 NCs, which have higher protein adsorption efficiency, than the CeO_2-25 NCs.

We next investigated whether nanoceria could protect INS-1 cells from oxidative stress induced by H_2O_2. INS-1 cells were cultured in the presence of 500 μM H_2O_2 at 37 °C for 1 h. The cells were then washed and placed in fresh medium containing CeO_2 NCs with varied size and concentrations for recovery. After such treatment for 24 h, CCK-8 assay was performed for viability analysis. As shown in Figure 7, the addition of H_2O_2 significantly increased cell apoptosis compared to the control, while the addition of 50 or 100 μg/mL CeO_2-5 NCs remarkably increased cell viability (from 30% to approximately 90%). It was worth noting that the CeO_2-25 NCs exhibited higher anti-apoptotic effects in a relative low concentration (10 and 25 μg/mL), which was consistent with their H_2O_2 quenching capability under cell culture conditions. The results indicated that the external environment, especially the protein corona formation, affects the catalytic antioxidant properties of nanoceria and thus affects the recovery of ROS-induced cell damage. These outcomes may provide guidance for the further medical applications of CeO_2 nanoparticles.

Conclusions

In summary, we have developed a facile and effective synthetic procedure to produce hydrophilic CeO_2 NCs by using an acetate assisted hydrothermal method. By employing different cerium precursors and reaction conditions, CeO_2 NCs of different sizes (5 and 25 nm) were obtained. The interactions of serum protein with nanoceria under *in vitro* cell culture conditions have also been investigated. The particle size and surface area of CeO_2 NCs have been found to have a great impact on the amount of the adsorbed proteins. In the meanwhile, the protein corona formed on the surface of nanoceria significantly alters their zeta potential, hydrodynamic radius, state of aggregation and H_2O_2 decomposition activity. *In vitro* toxicity studies showed the compatibility of nanoceria with INS-1 cells. Moreover, the concentration and hydrodynamic radius of CeO_2 NCs play key roles in determining the recovery of apoptotic INS-1 cells induced by H_2O_2. All these findings clearly demonstrate that CeO_2 NCs can function as excellent catalytic antioxidants and be promising candidates for further development in the treatment of ROS-mediated diabetes.

Acknowledgements

This work was supported by NSFC (Nos. 21425101, 21321001, 21371011, 21331001) and MOST of China (2014CB643800). We thank Mr. An-Dong Wang (CCME, PKU) for his help in DLS and zeta potential measurements. We also thank Prof. Xing Chen, Prof. Peng Chen, S. Engr. Rong-Hua Sun, Mr. Ze-Fan Li and Mr. Yi Yang (CCME, PKU) for their assistence in cell culture and imaging.

Notes and references

1 P. Zimmet, K. G. M. M. Alberti and J. Shaw, *Nature*, 2001, **414**, 782-787.
2 American Diabetes Association, *Diabetes Care*, 2014, **37 Suppl 1**, S81-S90.
3 D. R. Whiting, L. Guariguata, C. Weil and J. Shaw, *Diabetes Res. Clin. Pract.*, 2011, **94**, 311-321.
4 M. Valko, D. Leibfritz, J. Moncol, M. T. D. Cronin, M. Mazur and J. Telser, *Int. J. Biochem. Cell Biol.*, 2007, **39**, 44-84.
5 M. Bensellam, D. R. Laybutt and J.-C. Jonas, *Mol. Cell. Endocrinol.*, 2012, **364**, 1-27.
6 X. G. Lei and M. Z. Vatamaniuk, *Antioxid. Redox Sign.*, 2011, **14**, 489-503.
7 A. C. Maritim, R. A. Sanders and J. B. Watkins, *J. Biochem. Mol. Toxic.*, 2003, **17**, 24-38.
8 J. S. Johansen, A. K. Harris, D. J. Rychly and A. Ergul, *Cardiovasc. Diabetol.*, 2005, **4**, 5.
9 J. Kašpar, P. Fornasiero and M. Graziani, *Catal. Today*, 1999, **50**, 285-298.
10 J. Ke, J. W. Xiao, W. Zhu, H. Liu, R. Si, Y. W. Zhang and C. H. Yan, *J. Am. Chem. Soc.*, 2013, **135**, 15191-15200.
11 J. Ke, W. Zhu, Y. Jiang, R. Si, Y. J. Wang, S. C. Li, C. Jin, H. Liu, W. G. Song, C. H. Yan and Y. W. Zhang, *ACS Catal.*, 2015, **5**, 5164-5173.
12 L. Liao, H. X. Mai, Q. Yuan, H. B. Lu, J. C. Li, C. Liu, C. H. Yan, Z. X. Shen and T. Yu, *J. Phys. Chem. C*, 2008, **112**, 9061-9065.
13 M. Aguirre, M. Paulis and J. R. Leiza, *J. Mater. Chem. A*, 2013, **1**, 3155-3162.
14 A. Atkinson, S. Barnett, R. J. Gorte, J. T. S. Irvine, A. J. McEvoy, M. Mogensen, S. C. Singhal and J. Vohs, *Nat. Mater.*, 2004, **3**, 17-27.
15 H. Dong, S. R. Du, X. Y. Zheng, G. M. Lyu, L. D. Sun, L. D. Li, P. Z. Zhang, C. Zhang and C. H. Yan, *Chem. Rev.*, 2015, **115**, 10725-10815.
16 C. Korsvik, S. Patil, S. Seal and W. T. Self, *Chem. Commun.*, 2007, **10**, 1056-1058.

17 Y. Li, X. He, J. J. Yin, Y. Ma, P. Zhang, J. Li, Y. Ding, J. Zhang, Y. Zhao, Z. Chai and Z. Zhang, *Angew. Chem. Int. Ed.*, 2015, **127**, 1852-1855.
18 T. Pirmohamed, J. M. Dowding, S. Singh, B. Wasserman, E. Heckert, A. S. Karakoti, J. E. S. King, S. Seal and W. T. Self, *Chem. Commun.*, 2010, **46**, 2736-2738.
19 Y. Xue, Q. Luan, D. Yang, X. Yao and K. Zhou, *J. Phys. Chem. C*, 2011, **115**, 4433-4438.
20 A. Asati, S. Santra, C. Kaittanis and J. M. Perez, *ACS Nano*, 2010, **4**, 5321-5331.
21 J. Chen, S. Patil, S. Seal and J. F. McGinnis, *Nat. Nanotechnol.*, 2006, **1**, 142-150.
22 C. K. Kim, T. Kim, I.-Y. Choi, M. Soh, D. Kim, Y.-J. Kim, H. Jang, H.-S. Yang, J. Y. Kim, H.-K. Park, S. P. Park, S. Park, T. Yu, B.-W. Yoon, S.-H. Lee and T. Hyeon, *Angew. Chem. Int. Ed.*, 2012, **51**, 11039-11043.
23 S. M. Hirst, A. S. Karakoti, R. D. Tyler, N. Sriranganathan, S. Seal and C. M. Reilly, *Small*, 2009, **5**, 2848-2856.
24 K. L. Heckman, W. DeCoteau, A. Estevez, K. J. Reed, W. Costanzo, D. Sanford, J. C. Leiter, J. Clauss, K. Knapp, C. Gomez, P. Mullen, E. Rathbun, K. Prime, J. Marini, J. Patchefsky, A. S. Patchefsky, R. K. Hailstone and J. S. Erlichman, *ACS Nano*, 2013, **7**, 10582-10596.
25 S. Chigurupati, M. R. Mughal, E. Okun, S. Das, A. Kumar, M. McCaffery, S. Seal and M. P. Mattson, *Biomaterials*, 2013, **34**, 2194-2201.
26 A. Briggs, S. Corde, S. Oktaria, R. Brown, A. Rosenfeld, M. Lerch, K. Konstantinov and M. Tehei, *Nanomedicine*, 2013, **9**, 1098-1105.
27 C. Sicard, M. Perullini, C. Spedalieri, T. Coradin, R. Brayner, J. Livage, M. Jobbagy and S. A. Bilmes, *Chem. Mater.*, 2011, **23**, 1374-1378.
28 J. P. Giraldo, M. P. Landry, S. M. Faltermeier, T. P. McNicholas, N. M. Iverson, A. A. Boghossian, N. F. Reuel, A. J. Hilmer, F. Sen, J. A. Brew and M. S. Strano, *Nat. Mater.*, 2014, **13**, 400-408.
29 S. S. Lee, W. Song, M. Cho, H. L. Puppala, P. Nguyen, H. Zhu, L. Segatori and V. L. Colvin, *ACS Nano*, 2013, **11**, 9693-9703.
30 J. M. Dowding, S. Das, A. Kumar, T. Dosani, R. McCormack, A. Gupta, T. X. T. Sayle, D. C. Sayle, L. von Kalm, S. Seal and W. T. Self, *ACS Nano*, 2013, **7**, 4855-4868.
31 X. Liu, W. Wei, Q. Yuan, X. Zhang, N. Li, Y. Du, G. Ma, C. Yan and D. Ma, *Chem. Commun.*, 2012, **48**, 3141-3148.
32 Y. Zhang, K. B. Zhou, Y. W. Zhai, F. Qin, L. L. Pan and X. Yao, *RSC Adv.*, 2014, **4**, 50325-50330.
33 G. M. Lv, Y. J. Wang, R. Liu, L. D. Sun, Y. H. Huang, C. H. Yan, Sci Sin. Chim., 2013, **43**, 1309-1321.
34 D. C. Sayle, S. A. Maicaneanu and G. W. Watson, *J. Am. Chem. Soc.*, 2002, **124**, 11429-11439.
35 H. X. Mai, L. D. Sun, Y. W. Zhang, R. Si, W. Feng, H. P. Zhang, H. C. Liu and C. H. Yan, *J. Phys. Chem. B*, 2005, **109**, 24380-24385.
36 S. Yang and L. Gao, *J. Am. Chem. Soc.*, 2006, **128**, 9330-9331.
37 K. Kaneko, K. Inoke, B. Freitag, A. B. Hungria, P. A. Midgley, T. W. Hansen, J. Zhang, S. Ohara and T. Adschiri, *Nano Lett.*, 2007, **7**, 421-425.
38 S. Tenzer, D. Docter, J. Kuharev, A. Musyanovych, V. Fetz, R. Hecht, F. Schlenk, D. Fischer, K. Kiouptsi, C. Reinhardt, K. Landfester, H. Schild, M. Maskos, S. K. Knauer and R. H. Stauber, *Nat Nano.*, 2013, **8**, 772-781.
39 M. P. Calatayud, B. Sanz, V. Raffa, C. Riggio, M. R. Ibarra and G. F. Goya, *Biomaterials*, 2014, **35**, 6389-6399.
40 M. P. Monopoli, C. Aberg, A. Salvati and K. A. Dawson, *Nat. Nanotechnol.*, 2012, **7**, 779-786.
41 L. Treuel, S. Brandholt, P. Maffre, S. Wiegele, L. Shang and G. U. Nienhaus, *ACS Nano*, 2014, **8**, 503-513.
42 M. P. Monopoli, D. Walczyk, A. Campbell, G. Elia, I. Lynch, F. B. Bombelli and K. A. Dawson, *J. Am. Chem. Soc.*, 2011, **133**, 2525-2534.
43 W. Liu, J. Rose, S. Plantevin, M. Auffan, J. Y. Bottero and C. Vidaud, *Nanoscale*, 2013, **5**, 1658-1668.
44 E. Casals, T. Pfaller, A. Duschl, G. J. Oostingh and V. F. Puntes, *Small*, 2011, **7**, 3479-3486.
45 X. C. Jiang, L. D. Sun, W. Feng and C. H. Yan, *Cryst. Growth Des.*, 2004, **4**, 517-520.
46 Y. W. Zhang, X. Sun, R. Si, L. P. You and C. H. Yan, *J. Am. Chem. Soc.*, 2005, **127**, 3260-3261.
47 Q. Wu, F. Zhang, P. Xiao, H. S. Tao, X. Z. Wang, Z. Hu and Y. N. Lü, *J. Phys. Chem. C*, 2008, **112**, 17076-17080.
48 Z. Ji, X. Wang, H. Y. Zhang, S. J. Lin, H. Meng, B. B. Sun, S. George, T. Xia, A. E. Nel and J. I. Zink, *Acs Nano*, 2012, **6**, 5366-5380.
49 J. A. Dean. *Lange's Handbook of Chemistry*, 13th ed., McGraw Hill, Inc., New York, 1985.
50 P. Holgado, R. Alvarez and G. Munuera, *Appl. Surf. Sci.*, 2000, 161, 301-315.
51 R. Gilliss, J. Bentley and C. B. Carter, *Appl. Surf. Sci.*, 2005, **241**, 61-67.
52 Lijun, H. J. Wiesmann, A. R. Moodenbaugh, R. F. Klie, Z. Yimei, D. O. Welch and M. Suenaga, *Phys. Rev. B*, 2004, **69**, 125415-125419.
53 E. Nel, L. Madler, D. Velegol, T. Xia, E. M. V. Hoek, P. Somasundaran, F. Klaessig, V. Castranova and M. Thompson, *Nat. Mater.*, 2009, **8**, 543-557.
54 E. C. Cho, J. Xie, P. A. Wurm and Y. Xia, *Nano Lett.*, 2009, **9**, 1080-1084.
55 A. Lesniak, F. Fenaroli, M. P. Monopoli, C. Åberg, K. A. Dawson and A. Salvati, *ACS Nano*, 2012, **6**, 5845-5857.
56 W. Hu, C. Peng, M. Lv, X. Li, Y. Zhang, N. Chen, C. Fan and Q. Huang, *ACS Nano*, 2011, **5**, 3693-3700.
57 A. Asati, S. Santra, C. Kaittanis, S. Nath and J. M. Perez, *Angew. Chem. Int. Ed.*, 2009, **48**, 2308-2312.
58 Y. J. Wang, H. Dong, G. M. Lyu, H. Y. Zhang, J. Ke, L. Q. Kang, J. L. Teng, L. Sun, R. Si, J. Zhang, Y. J. Liu, Y. Zhang, Y. Huang and C. H. Yan, *Nanoscale*, 2015, **7**, 13981-13990.